Solution Conformation of the (−)-*trans-anti*-5-Methylchrysene−dG Adduct opposite dC in a DNA Duplex: DNA Bending Associated with Wedging of the Methyl Group of 5-Methylchrysene to the 3′-Side of the Modification Site†

Monique Cosman,‡ Rong Xu,§ Brian E. Hingerty,|| Shantu Amin,⊥ Ronald G. Harvey,# Nicholas E. Geacintov,§ Suse Broyde,Δ and Dinshaw J. Patel*,‡

Cellular Biochemistry and Biophysics Program, Memorial Sloan-Kettering Cancer Center, New York, New York 10021, Chemistry and Biology Departments, New York University, New York, New York 10003, Health Sciences Research Division, Oak Ridge National Laboratory, Oak Ridge, Tennessee 37831, American Health Foundation, Valhalla, New York 10595, and Ben May Institute, University of Chicago, Chicago, Illinois 60637

Received December 9, 1994; Revised Manuscript Received March 2, 1995⊗

ABSTRACT: This paper reports on NMR−molecular mechanics structural studies of the (−)-*trans-anti*-[MC]dG adduct positioned opposite dC in the sequence context of the d(C1-C2-A3-T4-C5-[MC]G6-C7-T8-A9-C10-C11)·d(G12-G13-T14-A15-G16-C17-G18-A19-T20-G21-G22) duplex [designated (−)-*trans-anti*-[MC]dG·dC 11-mer duplex]. This adduct is derived from the *trans* addition at C^4 of (−)-*anti*-1(*S*),2(*R*)-dihydroxy-3(*R*),4(*S*)-epoxy-1,2,3,4-tetrahydro-5-methylchrysene [(−)-*anti*-5-MeCDE] to the N^2 position of dG6 in this duplex sequence. The 5-methyl group is located adjacent to the MC(C^4) binding site, with these groups juxtaposed in a sterically crowded bay region in the adduct duplex. The 5-methylchrysenyl and the nucleic acid exchangeable and nonexchangeable protons were assigned following analysis of two-dimensional NMR data sets in H_2O and D_2O buffer solution. The solution structure of the (−)-*trans-anti*-[MC]dG·dC 11-mer duplex has been determined by incorporating DNA−DNA and carcinogen−DNA proton−proton distances defined by lower and upper bounds deduced from NOESY data sets as restraints in molecular mechanics computations in torsion angle space. The results establish that the [MC]dG6·dC17 base pair and flanking dC5·dG18 and dC7·dG16 base pairs retain Watson−Crick alignments upon adduct formation. The aromatic chrysenyl ring is positioned in the minor groove of a right-handed B-DNA helix and stacks predominantly over the sugar of the dC17 residue across from it on the unmodified complementary strand. The chrysenyl ring points toward the 3′-end of the modified strand with its 5-methyl group inserting between the modified [MC]dG6·dC17 and dC7·dG16 base pairs. The adduct duplex bends by ~47° as a result of the wedged insertion of the 5-methyl group from the minor groove face of the duplex. The solution structure of the (−)-*trans-anti*-[MC]dG·dC 11-mer duplex is compared with that of the corresponding (−)-*trans-anti*-[BP]dG·dC 11-mer [De los Santos et al. (1992) *Biochemistry 31*, 5245−5252] in which the [BP]dG adduct is derived from the binding of (−)-*anti*-BPDE [7(*S*),8(*R*)-dihydroxy-9(*R*),10(*S*)-epoxy-7,8,9,10-tetrahydrobenzo[*a*]pyrene] to the N^2 position of dG in the same DNA sequence context. Although the solution structures of the (−)-*trans-anti* stereoisomers of 5-methylchrysenyl-dG and benzo[*a*]pyrenyl-dG adducts opposite dC exhibit many features in common with each other, the [MC]-dG adduct which contains a bay region methyl group bends the DNA helix to a greater extent than in the corresponding [BP]dG adduct, which lacks a bay region methyl group. Carcinogen-induced bending effects may be important factors in the expression of the mutagenic potential of these [MC]dG lesions. Because of the stabilities of these lesions, site-directed mutagenesis studies are now feasible which should lead to new insights into the relationships between adduct structure, DNA structural distortions, and mutagenic specificity and activity.

Polycyclic aromatic hydrocarbons (PAH) are a class of potentially mutagenic and carcinogenic environmental pollutants (Lunde & Bjorseth, 1977; Wise et al., 1986). Subtle variations in structure can be accompanied by remarkable effects in biological activities. For example, methyl substitution of chrysene at the 5-position greatly enhances its tumorigenicity, while substitution at other positions does not markedly affect the intrinsically weak tumorigenicity of the parent compound (Hecht et al., 1974, 1986, 1987; Amin et al., 1991). The presence of the methyl group at the 5-position in 5-methylchrysene (5-MeC) is believed to play an important role in its carcinogenic activity (Hecht et al., 1979, 1985).

Like other PAH compounds (Miller, 1978; Singer & Grunberger, 1983; Conney, 1982; Harvey, 1991), 5-MeC is metabolically activated to highly reactive and potentially biologically active bay region diol epoxide derivatives (Hecht

† This research is supported by NIH Grant CA-46533 to D.J.P., by NIH CA-20851 and DOE Grant DE-FG02-88ER60405 to N.E.G., by NIH Grant CA-28038, NIH Grant RR-06458, and DOE Grant DE-FG02-90ER60931 to S.B., by DOE Contract DE-AC05-840R21400 with Martin-Marietta Energy Systems and DOE OHER Field Work Proposal ERKP931 to B.E.H., and by American Cancer Society Grant CN-22 to R.G.H.

‡ Memorial Sloan-Kettering Cancer Center.
§ Chemistry Department, New York University.
|| Oak Ridge National Laboratory.
⊥ American Health Foundation.
Ben May Institute, University of Chicago.
Δ Biology Department, New York University.

⊗ Abstract published in *Advance ACS Abstracts,* May 1, 1995.

0006-2960/95/0434-6247$09.00/0

et al., 1978, 1980, 1985, 1987; Amin et al., 1985). The ultimate biologically important metabolites of 5-MeC are the diastereomeric *anti*- and *syn*-1,2-dihydroxy-3,4-epoxy-1,2,3,4-tetrahydro-5-methylchrysene (*anti*- and *syn*-5-MeCDE). Each of these diastereomers can be resolved into a pair of enantiomers; for example, the two chiral stereoisomers of *anti*-5-MeCDE are the 1*R*,2*S*,3*S*,4*R*-((+)-*anti*-5-MeCDE) and the 1*S*,2*R*,3*R*,4*S*-((−)-*anti*-5-MeCDE) enantiomers.

The tumorigenic activity of *anti*-5-MeCDE in newborn mice and on mouse skin (Hecht et al., 1980, 1985, 1987) and its mutagenic activity in Chinese hamster V79 cells (Brookes et al., 1986), in the TA 100 strain of *Salmonella typhimurium* (Amin et al., 1986, 1988), and in the *supF* target gene of an SV40-based pS189 shuttle vector replicating in human cells (Bigger et al., 1990) have been studied. The (+)-*anti*-5-MeCDE enantiomer is significantly more tumorigenic than the (−)-enantiomer in the lung of newborn mice and in the mouse skin tumor model systems (Hecht et al., 1987; Melikian, 1988). In addition, the (+)-enantiomer is highly mutagenic while the chiral (−)-isomer is only weakly mutagenic in *S. typhimurium* TA 100 (Melikian et al., 1988). The molecular basis of these effects and the reasons for the influence of the methyl group are not yet understood (Hecht et al., 1986).

Both the mutagenic activities and the initiation of the tumorigenic process are believed to be associated with the covalent binding of the 5-MeCDE isomers to native DNA (Melikian et al., 1982, 1983, 1984, 1991; Reardon et al., 1987). The major DNA adducts obtained from the reaction of (±)-*anti*-5-MeCDE with calf thymus DNA (Melikian et al., 1984, 1988), nucleotides (Reardon et al., 1987), and single stranded oligodeoxyribonucleotides (Xu, 1994) arise from the *trans* opening of the epoxide ring by the exocyclic amino group of deoxyguanosine (N^2-dG) at the C^4 position (modified guanine designated as [MC]dG). The differences in the biological end points associated with each of these two stereoisomeric lesions may well be associated with the three-dimensional structural features of the DNA adducts derived from (+)- and (−)-*anti*-5-MeCDE. The recent availability of homogeneous (+)- and (−)-*trans-anti*-[MC]-dG oligodeoxyribonucleoside adducts in sufficient quantities needed for two-dimensional NMR structural studies (Xu, 1994) provides us with the opportunity to study solution structures of adducts derived from these two *anti*-5-MeCDE enantiomers having strikingly different biological activities. The conformations of adducts derived from the covalent binding of (+)-*anti*-5-MeCDE and (−)-*anti*-5-MeCDE to native DNA by UV spectroscopic methods have been previously studied, but the orientational characteristics of the (−)-*anti*-5-MeCDE-DNA adducts could not be established, most likely because of a multiplicity of adducts (Geacintov et al., 1990). The results of this investigation represent the first results on the conformational characteristics of the adduct derived from the chemical reaction of a methylated PAH diol epoxide with DNA.

In this current contribution, we present two-dimensional NMR−molecular mechanics studies of the (−)-*trans-anti*-[MC]dG adduct **1** positioned opposite dC in the same DNA sequence **2** as used previously in the structural studies of the three stereospecific benzo[*a*]pyrenyl [BP]dG duplex adducts (Cosman et al., 1992, 1993a; De los Santos et al., 1992). Our results show that the structures of the (−)-*trans-anti*-[MC]dG•dC 11-mer duplex and analogous benzo[*a*]pyrenyl (−)-*trans-anti*-[BP]dG•dC 11-mer duplex (De los Santos et al., 1992) have several common features. The steric configuration and orientation of the substituents on the benzylic ring are identical in both adducts, but the benzo[*a*]pyrenyl moiety has an additional aromatic ring and lacks a methyl group. The aromatic (either chrysenyl or pyrenyl) ring in both the 5-methylchrysenyl and benzo[*a*]pyrenyl (−)-*trans-anti* adducts is located in the minor groove, is directed toward the 3′-end of the modified strand of a minimally perturbed B-DNA duplex, and stacks predominantly over the dC17 residue on the unmodified strand. However, the bay region methyl group wedges into the helix, thereby bending the helix to a greater degree than in the case of the (−)-*trans-anti*-[BP]dG adduct in which the methyl group is absent.

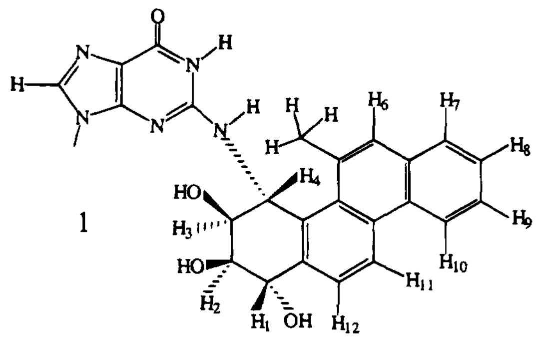

1

C1 - C2 - A3 - T4 - C5 - *G6 - C7 - T8 - A9 - C10 - C11

G22 - G21 - T20 - A19 - G18 - C17 - G16 - A15 - T14 - G13 - G12

2

MATERIALS AND METHODS

Preparation of (−)-trans-anti-[MC]dG•dC 11-mer Duplex. The racemic (±)-*anti*-5-MeCDE was synthesized following published procedures (Pataki et al., 1983; Amin et al., 1984; Harvey et al., 1986). The synthesis of the [MC]dG covalent adducts in the d(C-C-T-A-C-G-C-T-A-C-C) sequence was carried out starting with racemic *anti*-5-MeCDE using previously described methods (Cosman et al., 1990) and will be described in detail elsewhere (Xu et al., in preparation). Briefly, the (−)-*trans-anti*-[MC]dG containing 11-mer (retention time at 32 min) was separable from the (+)-*trans-anti* stereoisomer (retention time at 38 min) by preparative HPLC on a C18 ODS Hypersil column using a 20 mM phosphate, pH 6.8 buffer/methanol linear gradient, 16% to 19% (10 min) and 19% to 22% (50 min), with a 3 mL/min flow rate. The ratio of the integrated areas of the HPLC elution peaks of the (−)-*trans-anti*-[MC]dG to (+)-*trans-anti*-[MC]dG adducts was about 1:1. In order to establish the identity of the adduct, the modified oligomer strands were degraded with snake venom phosphodiesterase I (Pharmacia LKB Biotechnology Inc., Piscataway, NJ) and bacterial alkaline phosphatase (Sigma Chemical Co., St. Louis, MO) to the nucleoside level (Cosman et al., 1990). The base composition and stereochemical features of the modified mononucleosides were characterized using methods described by Reardon et al. (1987) using CD and UV absorption spectroscopy. The modified stereoisomerically pure d(C-C-A-T-C-[MC]G-C-T-A-C-C) strand was annealed to its

complementary unmodified d(G-G-T-A-G-C-G-A-T-G-G) strand at 70 °C by monitoring the stoichiometry of single proton resonances in both strands.

NMR Experiments. A combination of through-space nuclear Overhauser effect (NOESY) and through-bond correlated (COSY, TOCSY) two-dimensional spectra were recorded on approximately 5 mg of the (−)-*trans-anti*-[MC]-dG•dC 11-mer duplex in 0.6 mL of 0.1 M NaCl, 10 mM phosphate, pH 7.0 aqueous buffer and analyzed in order to assign the carcinogen and nucleic acid protons. All experiments were carried out using a Varian Unity Plus 600 MHz instrument in the States-TPPI mode (Marion et al., 1989) with a 2.0 s relaxation delay between scans. The temperature of the sample was calibrated with an external methanol sample. The NOESY spectrum (150 ms mixing time) of the adduct duplex in H_2O buffer at 1 °C was collected using a jump−return pulse for solvent suppression, and NOESY spectra (50, 100, 150, 200, and 300 ms mixing times) were collected in D_2O buffer at 25 °C. The through-bond TOCSY data sets in D_2O buffer were recorded at spin lock times of 40 and 80 ms at 25 °C. The proton−phosphorus correlation spectrum of the adduct duplex in D_2O buffer, pH 7.0 was recorded at 25 °C, using the method described in Sklenar et al. (1986) with sweep widths set to 6 ppm in both $\omega 1$ and $\omega 2$, and with a 1.3 s presaturation of the HDO signal. The phosphorus spectrum was referenced with an external 10% (v/v) trimethyl phosphate (TMP) sample.

Several factors went into the conversion of the NOE intensities into the distance bounds used for the structure determination of the adduct duplex. Distance restraints involving nonexchangeable protons were estimated from NOE buildup curves of NOESY spectra recorded at 50, 100, 150, 200, and 300 ms on the adduct duplex in D_2O. The interproton distance calculations were based on the isolated two-spin approximation using the dT(NH3)−dA(H2) fixed distance of 2.92 Å for the NOESY spectrum in H_2O and the dC(H6)−dC(H5) fixed distance of 2.45 Å and the dT(H6)−dT(5-CH_3) fixed distance of 2.78 Å for the NOESY data sets in D_2O solution. The choice of upper and lower bound ranges on the estimated distances depended on the resolution of the cross peaks in the contour plots. The base proton to sugar H1′ NOE cross-peaks in the shortest mixing time NOESY data set in D_2O were evaluated to qualitatively differentiate between *syn* (strong NOE) and *anti* (weak NOE) glycosidic torsion angles (Patel et al., 1982).

The proton−proton vicinal coupling constants among sugar protons were analyzed from phase-sensitive COSY spectra to qualitatively distinguish between the C3′-*endo* and C2′-*endo* family of sugar puckers in the (−)-*trans-anti*-[MC]-dG•dC 11-mer duplex. The relative intensity of the NOE cross-peaks between base protons and their own and 5′-flanking sugar H2′, H2″, and H3′ protons was used to qualitatively distinguish between the A and B family of helices for the modified duplex (van der Ven & Hilbers, 1988).

The three-bond proton−proton vicinal coupling constant patterns for benzylic ring protons of the [MC]dG adduct in the adduct duplex were computed using the program CHORDS (Majumdar & Hosur, 1992) to constrain torsion angles linking MC(H1)−MC(H2) and MC(H3)−MC(H4) proton pairs.

Molecular Mechanics Computations. Minimized potential energy calculations were carried out with DUPLEX, a molecular mechanics program for nucleic acids that performs potential energy minimizations in the reduced variable domain of torsion angle space (Hingerty et al., 1989).

Force field parameters, including partial charges, for the (−)-*trans-anti*-[MC]dG adduct were the same as those employed for the (−)-*trans-anti*-[BP]dG adduct (Hingerty & Broyde, 1985; Singh et al., 1991) except that new partial charges had to be computed for the chrysenyl moiety and for the linkage site (Supplementary Figure S1). This was accomplished for the (−)-*trans-anti*-[MC]dG adduct with the CNDO module of the program CHEM-X (Chemical Design, Ltd., Mahwah, NJ) which yields partial charges compatible with the set employed in DUPLEX (Ornstein & Rein, 1979). The geometry (bond lengths, bond angles, and dihedral angles) of the (−)-*trans-anti*-[MC]dG adduct was generated from that employed for the [BP]dG adducts (Hingerty & Broyde, 1985; Singh et al., 1991) by computer graphics on a Silicon Graphics Personal Iris Model 4D-35 with the program INSIGHT (Biosym Technologies, Inc., Parsippany, NJ). The conformation of the benzylic ring was in the distorted half-chain form with the MC(H3) and MC(H4) protons in the diequatorial domain and MC(H1) and MC(H2) protons in the diaxial domain (Neidle et al., 1982), as the analysis of the COSY cross-peaks (Results section) had shown this to be the correct orientation. The constructed model was energy minimized with DISCOVER (Biosym Technologies) using the default parameters and potential energy function with a conjugate gradient minimization and a rotor constraint for the chrysenyl carbon 5-methyl to carbon in the ring bond. The rotor constraint allowed the MC(5-CH_3) group to rotate during the minimization, since this rotation had been indicated by the data. The resulting structure was then implemented within DUPLEX.

To locate minimum energy conformations with interproton distances suggested from the experimental NMR data, pseudo-potentials (permitting upper and lower bound restraints) were added to the energy, as described previously (Norman et al., 1989; Schlick et al., 1990). Briefly, the following functions were used.

$$F_N = W_N \sum_1^n (d - d_N)^2 \quad (1)$$

$$F_{NN} = W_{NN} \sum_1^n (d - d_{NN})^2 \quad (2)$$

The W's are adjustable weights (in the range of 10−30 kcal/(mol•Å^2)), d is the current value of the interproton distance, d_N is a target upper bound, and d_{NN} a target lower bound. The summation is over all n NMR derived distance bounds. Equation 1 is implemented when d is greater than d_N, and eq 2 is implemented when d is less than d_{NN}. F_N and F_{NN} can also be employed as goodness-of-fit indices to compare the quality of computed structures with respect to the NMR data. In this case d is the distance achieved in the model. All penalty functions were released in the last minimization steps to yield unrestrained final structures that are energy minima.

Computations were carried out at the Department of Energy's National Energy Research Supercomputer Center and the National Science Foundation's San Diego Supercomputer Center.

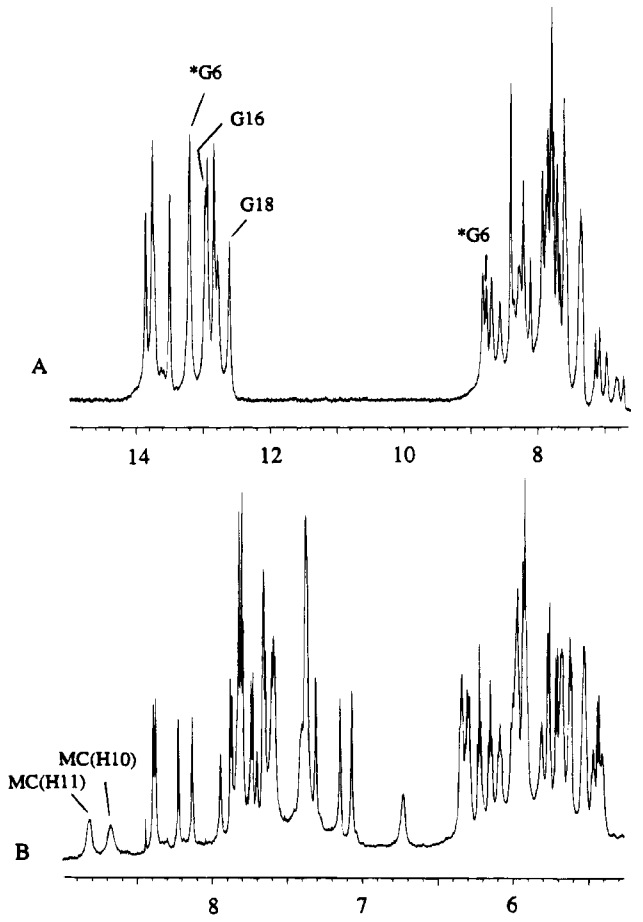

FIGURE 1: The proton NMR spectra of the (−)-*trans-anti*-[MC]-dG•dC 11-mer duplex in 0.1 M NaCl, 10 mM phosphate, and 0.1 mM EDTA, aqueous solution, pH 7.0. (A) The imino proton spectrum (7.0−15.0 ppm) in H_2O buffer at 1 °C and (B) the nonexchangeable proton spectrum (5.2−8.9 ppm) in D_2O buffer at 25 °C. Selective imino, amino, and chrysenyl proton assignments are recorded over the spectrum.

RESULTS

Exchangeable Nucleic Acid Protons. The exchangeable proton NMR spectrum (6.8−15.0 ppm) of the (−)-*trans-anti*-[MC]dG•dC 11-mer duplex in H_2O buffer, pH 7.0 at 1 °C, is plotted in Figure 1A. Several partially resolved imino protons are detected between 12.5 and 14.0 ppm and have been assigned following analysis of the NOESY spectrum of the adduct duplex in H_2O buffer, pH 7.0 at 1 °C, using standard procedures (reviewed in Patel et al., 1987; van de Ven & Hilbers, 1988). We can readily follow the NOE connectivities between imino protons on adjacent base pairs from dG13 toward one end of the helix to dG21 toward the opposite end in the expanded NOESY (150 ms mixing time) contour plot of the symmetrical 12.4−14.0 ppm region (Figure 2A). We note, however, that the intensity of the cross-peak between the neighboring imino protons of [MC]-dG6 and dG16 is weak (peak D, Figure 2A) in comparison to the cross-peak between the adjacent imino protons of [MC]-dG6 and dG18 (peak E, Figure 2A) in the d(C5-[MC]G6-C7)•d(G16-C17-G18) segment of the adduct duplex.

An expanded NOESY contour plot correlating the NOEs between the imino protons (12.4−14.0 ppm) and the base and amino protons (5.6−8.9 ppm) is plotted in Figure 3A. The observed NOE patterns establish Watson−Crick pairing at all dA•dT pairs (characterized by a NOE between thymine

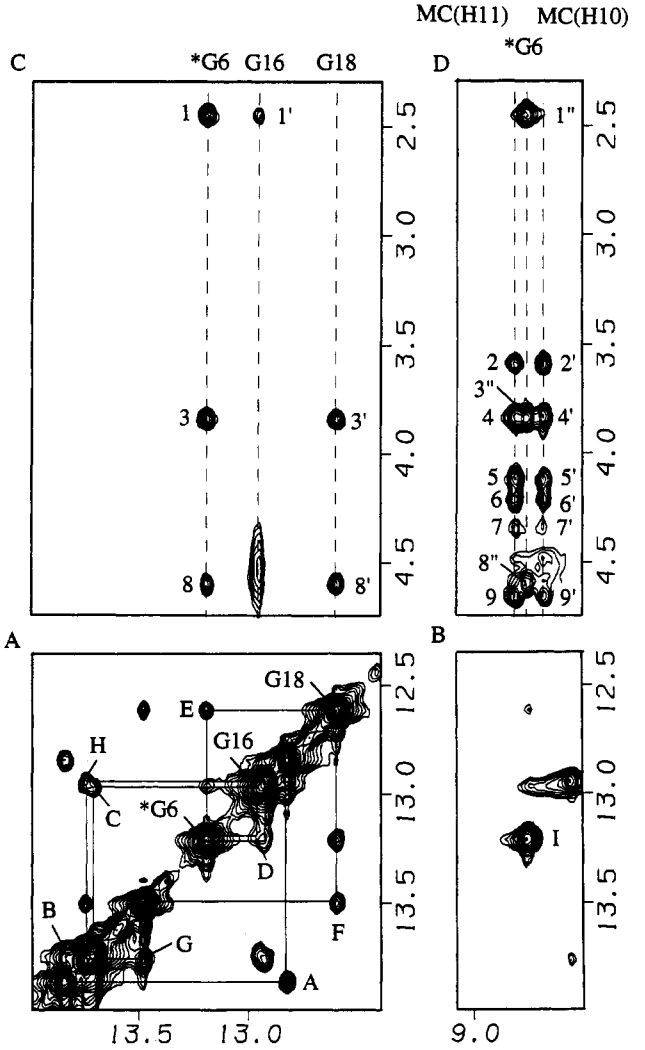

FIGURE 2: Expanded NOESY (150 ms mixing time) contour plots of the (−)-*trans-anti*-[MC]dG•dC 11-mer duplex in H_2O buffer at 1 °C. (A) NOE connectivities in the symmetrical 12.4−14.0 ppm region. The imino assignments of the central d(T4-C5-[MC]G6-C7-T8)•d(A15-G16-C17-G18-A19) segment are labeled along the diagonal. The lines trace the NOE connectivities between adjacent base pairs starting at G13 toward one end of the helix and proceeding to G21 toward the other end of the helix. The cross-peaks A−H are assigned as follows: A: dG13(NH1)−dT14(NH3); B: dT14(NH3)−dT8(NH3); C: dT8(NH3)−dG16(NH1); D: dG16-(NH1)−[MC]dG6(NH1); E: [MC]dG6(NH1)−dG18(NH1); F: dG18(NH1)−dT4(NH3); G: dT4(NH3)−dT20(NH3); H: dT20-(NH3)−dG21(NH1). (B) NOE connectivities between the imino protons (12.4−14.0 ppm) and [MC]dG6(NH2), MC(H10), and MC-(H11) protons (8.5−9.0 ppm). Cross-peak I is assigned as [MC]-dG6(NH1)−[MC]dG6(NH2). NOE connectivities (C) from the imino (12.4−14.0 ppm) and (D) from the [MC]dG6(NH2), MC-(H10), and MC(H11) protons (8.5−9.0 ppm) to the 5-methylchrysenyl and the sugar H1′, H4′, H5′, H5″ protons (2.3−4.8 ppm). The cross-peaks identifying carcinogen−DNA NOEs are numbered 1−9 and are assigned as follows: 1,1′,1″: MC(5-CH_3)−[MC]dG6-(NH1), dG16(NH1), [MC]dG6(NH2); 2,2′: C17(H4′)−MC(H11), MC(H10); 3,3′,3″: MC(H2)−[MC]dG6(NH1), dG18(NH1), [MC]-dG6(NH2); 4,4′: C17(H1′/H5′/H5″)−MC(H11), MC(H10); 5,5′: G18(H5′/H5″)−MC(H11), MC(H10); 6,6′: G18(H5′/H5″)−MC-(H11), MC(H10); 7,7′: G6(H4′)−MC(H11), MC(H10); 8,8′,8″: MC(H3)−[MC]dG6(NH1), dG18(NH1), [MC]dG6(NH2); 9,9′: dG18(H4′)−MC(H11), MC(H10).

imino and adenine H2 protons across the pair) and all dG•dC pairs (characterized by a NOE between guanine imino and cytosine amino protons across the pair) as shown for the [MC]dG6•dC17 base pair (peaks A and A′, Figure 3A) and

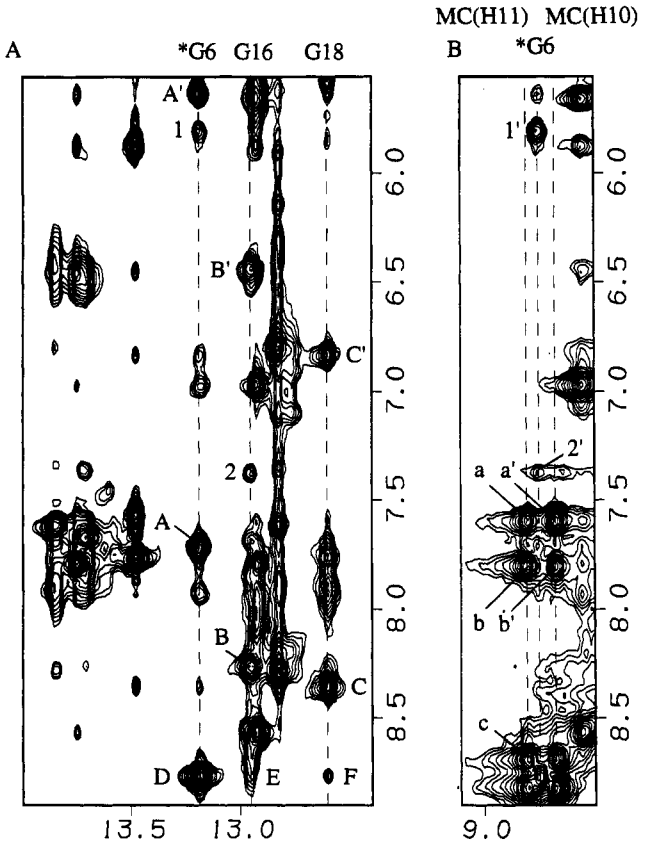

FIGURE 3: Expanded NOESY (150 ms mixing time) contour plots of the (−)-*trans-anti*-[MC]dG·dC 11-mer duplex in H_2O buffer at 1 °C. NOE connectivities (A) from the imino protons (12.4−14.0 ppm) and (B) from the [MC]dG6(NH2), MC(H10), and MC(H11) protons (8.5−9.0 ppm) to the base and amino DNA protons and 5-methylchrysenyl protons (5.6−8.9 ppm). The cross-peaks A−F are assigned as follows. A,A′: [MC]dG6(NH1)−dC17(NH_2-4b,e); B,B′: dG16(NH1)−dC7(NH_2-4b,e); C,C′: dG18(NH1)−dC5(NH_2-4b,e); D: [MC]dG6(NH1)−[MC]dG6(NH2); E: dG16(NH1)−[MC]dG6(NH2); F: dG18(NH1)−[MC]dG6(NH2). The cross-peaks identifying carcinogen−DNA NOEs are numbered 1 and 2 and are assigned as follows: 1,1′: MC(H4)−[MC]dG6(NH1), [MC]-dG6(NH2); 2,2′: MC(H7)−dG16(NH1), [MC]dG6(NH2) and/or C7(H6)−dG16(NH1), [MC]dG6(NH2). The cross-peaks labeled a−c identify NOEs between 5-methylchrysenyl protons and are assigned as follows: a,a′: MC(H9)−MC(H11), MC(H10); b,b′: MC(H12)−MC(H11), MC(H10); c: MC(H11)−MC(H10).

flanking dC7·dG16 (peaks B and B′, Figure 3A) and dC5·dG18 (peaks C and C′, Figure 3A) base pairs.

A strong NOE between the imino proton (13.21 ppm) of [MC]dG6(NH1) and an exchangeable proton at 8.79 ppm (peak I, Figure 2B, and peak D, Figure 3A) permits assignment of this resonance to the amino proton of [MC]-dG6 in the adduct duplex. The observed downfield shifts of both the NH1 and NH2 protons of the modified guanine of [MC]dG6 confirm that they participate in hydrogen-bonding interactions with the partner dC17 residue. For comparison, the chemical shift ranges for related cytidine amino protons are 7.7−8.6 ppm for the hydrogen-bonded protons and 5.7−7.1 ppm for the exposed protons in Watson−Crick dG·dC base pairs in the adduct duplex. In addition, NOEs are observed between the [MC]dG6[NH2] proton and adjacent imino protons of dG16 and dG18 (peaks E and F, respectively, Figure 3A) in the adduct duplex.

The exchangeable imino and amino proton chemical shifts for the central d(T4-C5-[MC]G6-C7-T8)·d(A15-G16-C17-G18-A19) segment of the (−)-*trans-anti*-[MC]dG·dC 11-mer duplex are listed in Table 1 and for the entire adduct duplex in Supplementary Table S1.

Table 1: Proton Chemical Shifts of the d(T4-C5-[MC]G6-C7-T8)·d(A15-G16-C17-G18-A19) Segment of the (−)-*trans-anti*-[MC]dG·dC 11-mer Duplex in Aqueous Buffer

Exchangeable Proton Chemical Shifts, ppm, 1 °C

	G(NH1)	T(NH3)	C(NH_2-4)	G(NH_2-2)
dT4·dA19		13.50		
dC5·dG18	12.61		6.85,[a] 8.38[b]	
[MC]dG6·dC17	13.21		5.6,[a] 7.74[b]	8.79
dC7·dG16	12.97		6.45,[a] 8.28[b]	
dT8·dA15		13.74		

Nonexchangeable Proton Chemical Shifts, ppm, 25 °C

	H8/H6	H2/H5/CH_3	H1′	H2′,H2″	H3′	H4′
dT4	7.17	1.45	5.95	2.03, 2.49	4.90	4.35
dC5	7.40	5.65	5.80	1.81, 2.22	4.87	4.06
[MC]dG6	7.97		6.38	2.65, 2.90	5.06	4.41
dC7	7.43	5.56	5.96	2.07, 2.44	4.81	4.06
dT8	7.40	1.73	5.96	2.13, 2.44	4.84	3.80
dA15	8.16	7.69	6.12	2.66, 2.84	5.08	4.41
dG16	7.60		5.51	2.20, 2.20	4.85	4.24
dC17	6.76	4.99	3.86	1.06, 1.67	4.52	3.59
dG18	7.73		5.56	2.69, 2.79	5.06	4.65
dA19	8.25	7.83	6.32	2.60, 2.94	5.11	4.58

[a] Exposed amino proton. [b] Hydrogen-bonded amino proton.

Nonexchangeable Nucleic Acid Protons. The proton NMR spectrum (5.3−9.0 ppm) of the (−)-*trans-anti*-[MC]dG·dC 11-mer duplex in D_2O buffer, pH 7.0 at 25 °C, is plotted in Figure 1B. We observe narrow nonexchangeable base and sugar H1′ protons except for two 5-methylchrysenyl protons at 8.68 and 8.82 ppm which are somewhat broadened in the spectrum. An expanded NOESY (300 ms mixing time) contour plot correlating the base protons (6.6−8.9 ppm) and the sugar H1′ protons (3.4−6.4 ppm) of the (−)-*trans-anti*-[MC]dG·dC 11-mer duplex at 25 °C is plotted in Figure 4. All the DNA base and sugar protons, with the exception of superpositioned sugar H5′,5″ protons, have been assigned following analysis of through-space NOESY data sets and through-bond COSY and TOCSY data sets of the adduct duplex in D_2O buffer at 25 °C using standard nucleic acid assignment procedures (Hare et al., 1983). Sequential NOEs between the base (purine H8 or pyrimidine H6) protons and their own and 5′-flanking sugar H1′ protons along the chain are traced from dT4 to dT8 on the modified strand (solid line) and from dA15 to dA19 on the unmodified complementary strand (dashed line) in Figure 4. We note that the cross-peak between the dG16(H1′) and dC17(H6) protons (boxed peak a, Figure 4) is much stronger than the cross-peak between the dC17(H1′) and dG18(H8) protons (boxed peak b, Figure 4) in the d(G16-C17-G18) central segment of the unmodified strand located opposite the lesion site. The base and sugar H1′ proton assignments have been confirmed by cross checks in other regions of the NOESY contour plot, as well as the corresponding COSY and TOCSY plots which have also yielded a complete set of sugar H2′, H2″, H3′, and H4′ proton assignments. The nonexchangeable proton chemical shifts for the central d(T4-C5-[MC]G6-dC7-T8)·d-(A15-G16-C17-G18-A19) segment are listed in Table 1 and for the entire adduct duplex in Supplementary Table S2.

We have also computed the exchangeable and nonexchangeable proton chemical shift changes on proceeding from the control duplex to the adduct duplex for the central d(T4-C5-[MC]G6-C7-T8)·d(A15-G16-C17-G18-A19) segment, and

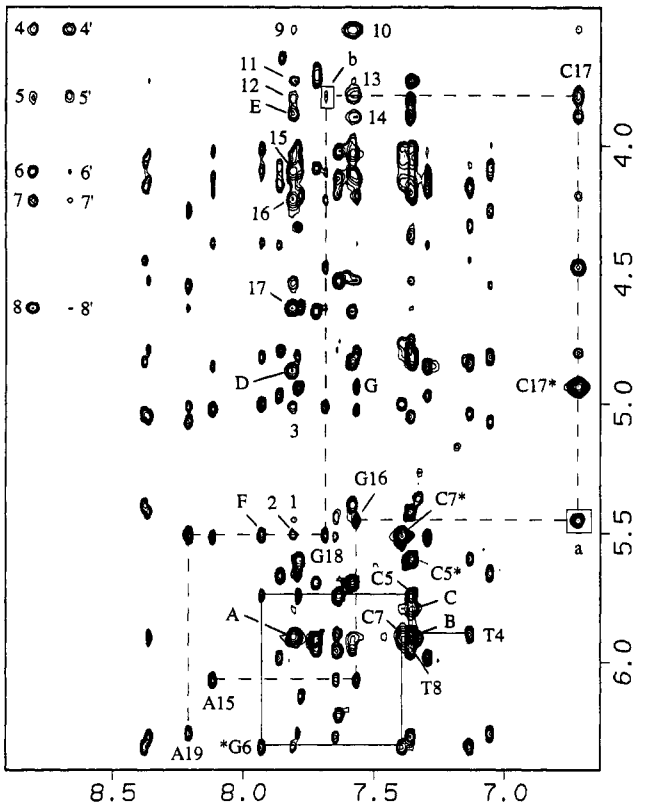

FIGURE 4: Expanded NOESY (300 ms mixing time) contour plot of the (−)-*trans-anti*-[MC]dG·dC 11-mer duplex in D_2O buffer at 25 °C, establishing distance connectivities between the base (purine H8 and pyrimidine H6) protons (6.6−8.9 ppm) and the sugar H1′ and cytosine H5 protons (3.4−6.4 ppm). The NOE connectivities between the base and their own and 5′-flanking sugar H1′ protons are traced from dT4 to dT8 on the modified strand (solid line) and from dA15 to dA19 on the unmodified strand (dashed line). The cross-peaks between cytidine H5 and H6 protons are designated by *. The cross-peak between G16(H1′) and C17(H6) protons is boxed and labeled "a", and the weak cross-peak between dC17-(H1′) and dG18(H8) protons is boxed and labeled "b". The cross-peaks labeled A−E identify NOEs between 5-methylchrysenyl protons and are assigned as follows: A: MC(H6)−MC(H8); B: MC(H6)−MC(H7); C: MC(H4)−MC(H7); D: MC(H1)−MC-(H12); E: MC(H2)−MC(H12). The cross-peaks F and G identify NOEs between adjacent DNA residues: F: [MC]dG6(H8)−dC7-(H5); G: dG16(H8)−dC17(H5). The cross-peaks numbered 1−17 identify carcinogen−DNA NOEs and are assigned as follows: 1: dG16(H1′)−MC(H8); 2: dG18(H1′)−MC(H12); 3: dG18(H3′)−MC(H12); 4,4′: dC17(H4′)−MC(H11), MC(H10); 5,5′: dC17(H1′/H5′,H5″)−MC(H11), MC(H10); 6,6′: dG18(H5′/H5″)−MC(H11), MC(H10); 7,7′: dG18(H5′/H5″)−MC(H11), MC(H10); 8,8′: dG18-(H4′)−MC(H11), MC(H10); 9: dC17(H4′)−MC(H8); 10: dC17-(H4′)−MC(H9); 11: dT8(H4′)−MC(H8); 12: dC17(H1′/H5′/H5″)−MC(H12); 13: dC17(H1′/H5′/H5″)−MC(H9); 14: dC17-(H5′,H5″)−MC(H9); 15: dG18(H5′/H5″)−MC(H12); 16: dG18-(H5′/H5″)−MC(H12); 17: dG18(H4′)−MC(H12).

these shift differences are listed in Supplementary Table S3. Small downfield shifts are observed for the imino protons of [MC]dG6 (+0.38 ppm) and dG16 (+0.23 ppm) while moderate upfield shifts are found for the exposed (−0.63 ppm) and hydrogen-bonded (−0.41 ppm) amino protons of dC17 on adduct formation. In addition, moderate to large upfield chemical shifts are observed for the minor groove H1′ (−1.72 ppm), H2″ (−0.61 ppm), and H4′ (−0.49 ppm) sugar protons, as well as the major groove H6 (−0.42 ppm) and H2′ (−0.77 ppm) base and sugar protons of dC17 upon adduct formation (Table S3). The nonexchangeable protons of the remaining residues flanking the lesion site in the d(C5-[MC]G6-C7)·d(G16-C17-G18) segment of the adduct duplex exhibit small to moderate shifts. In particular, the H1′ (−0.16 ppm), H2′ (−0.25 ppm), and H2″ (−0.38 ppm) sugar protons of dG16 are shifted upfield while the minor groove H1′ (+0.53 ppm) and H2″ (+0.20 ppm) sugar protons of the modified guanosine of [MC]dG6 are shifted downfield on adduct formation (Table S3).

Nonexchangeable 5-Methylchrysenyl Protons. The non-exchangeable 5-methylchrysenyl protons were assigned from an analysis of the through-bond and through-space connectivities in the (−)-*trans-anti*-[MC]dG·dC 11-mer duplex. The chemical shifts of the aromatic chrysenyl protons resonate between 7.5 and 9.0 ppm as shown in Figure 5, with the exception of the MC(H6) proton (5.92 ppm), which exhibits an approximately 1.5 ppm upfield shift compared to the other protons located on the aromatic ring (Figure 5). Although the 5-methyl group is located in the sterically hindered bay region, the 5-methyl protons are found to rotate freely about the methyl carbon (C^M) to the carbon in the ring (C^5) bond since they resonate at an average value of 2.45 ppm. The 5-methylchrysenyl proton chemical shifts are given in the caption of Figure 5 and are compared with those of the analogous benzo[*a*]pyrenyl protons in the (−)-*trans-anti*-[BP]-dG·dC 11-mer duplex (De los Santos et al., 1992) in Figure 5.

The broad MC(H10) (8.68 ppm) and MC(H11) (8.82 ppm) protons are located in the second unsubstituted bay region of the 5-methylchrysenyl aromatic ring **1** and are thus positioned close to one another in space (NOE peak C, Figure 3B) in the plane of each other's aromatic ring. The MC-(H10) and MC(H11) protons resonate ~0.5 ppm downfield relative to the chemical shifts of the other aromatic chrysenyl ring protons (Figure 5).

There is good agreement between the experimental coupling cross-peak patterns and their simulated counterparts based on three-bond vicinal proton−proton coupling constant values of ^3J(H1,H2) = 9.0 ± 0.2 Hz, ^3J(H2,H3) = 3.0 ± 0.5 Hz, and ^3J(H3,H4) = 5.5 ± 0.2 Hz. A strong experimental phase-sensitive COSY coupling cross-peak (peak B, Supplementary Figure S2A) is observed for the coupled MC(H1)−MC(H2) benzylic ring protons compared to the medium and weak intensity COSY cross-peaks observed between MC(H3)−MC(H4) protons and MC(H2)−MC(H3) protons (peaks C and A, respectively, Figure S2A). In addition, the 50 ms mixing time NOE cross-peak between the MC(H1)−MC(H2) protons (peak B, Figure S2B) is weaker than that seen for the MC(H3)−MC(H4) and MC-(H2)−MC(H3) proton pairs (peaks C and A, respectively, Figure S2B). These results are consistent with the distorted half-chair conformation of the benzylic ring where MC(H1) and MC(H2) protons adopt pseudo-diaxial orientations while the MC(H3) and MC(H4) protons adopt pseudo-diequatorial orientations.

Carcinogen−DNA NOEs. A set of 33 carcinogen−DNA NOEs including 11 involving exchangeable protons have been identified in the NOESY spectrum of the (−)-*trans-anti*-[MC]dG·dC 11-mer duplex (Table 2). Several of the carcinogen−DNA NOEs are labeled by numbers in the expanded NOESY (150 ms mixing time) contour plots of exchangeable protons of the adduct duplex in H_2O solution (Figures 2 and 3) and in the expanded NOESY (300 ms mixing time) contour plots of nonexchangeable protons of the adduct duplex in D_2O buffer (Figure 4). The cross-peak

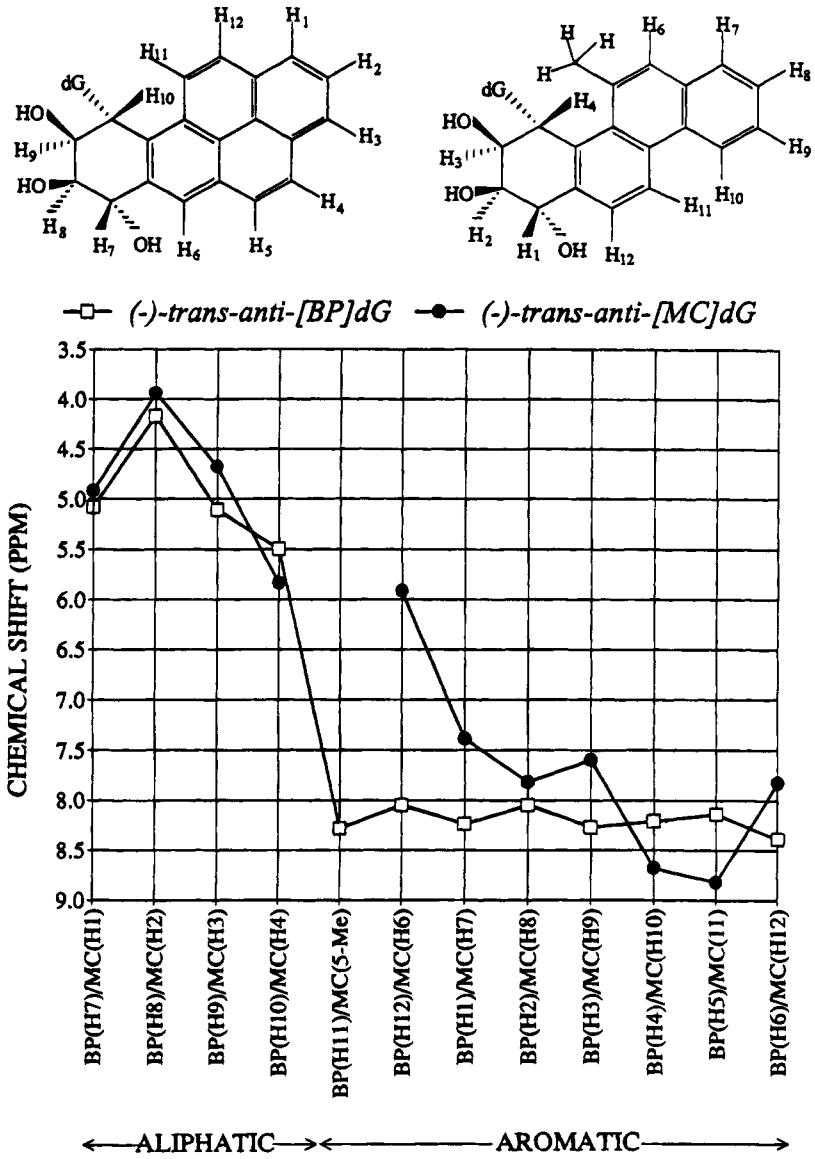

FIGURE 5: A plot comparing the 5-methylchrysenyl ring proton chemical shifts in the (−)-*trans-anti*-[MC]dG·dC 11-mer and the pyrenyl ring proton chemical shifts in the (−)-*trans-anti*-[BP]dG·dC 11-mer duplexes in D_2O buffer at 25 °C. Their structures and numbering schemes are shown above the plot. The chemical shift values in ppm for the 5-methylchrysenyl protons are as follows: MC(H1): 4.92; MC(H2): 3.94; MC(H3): 4.68; MC(H4): 5.84; MC(5-CH_3): 2.45; MC(H6): 5.92; MC(H7): 7.39; MC(H8): 7.82; MC(H9): 7.60; MC(H10): 8.68; MC(H11): 8.82; and MC(H12): 7.83.

assignments are listed in the captions of Figures 2−4. The corresponding carcinogen−DNA distance restraints defined by lower and upper bounds for the central d(C5-[MC]G6-C7)·d(G16-C17-G18) segment, which define the alignment of the (−)-*trans-anti*-[MC]dG adduct along the DNA helix, are listed in Table 2.

The majority of the carcinogen−DNA NOEs observed for the adduct duplex involve the minor groove sugar (H1′, H2″, and H4′) protons of the d([MC]G6-C7)·d(G16-C17-G18) segment (Table 2) positioning the 5-methylchrysenyl ring in the minor groove of the duplex. The observed distribution of carcinogen−DNA NOEs for the adduct duplex (Table 2) defines both the directionality of the 5-methylchrysenyl ring along the minor groove of the DNA helix, as well as the alignment of the two long edges of the 5-methylchrysenyl ring relative to the two strands of the duplex.

Phosphorus Spectra. The proton decoupled phosphorus spectrum of the (−)-*trans-anti*-[MC]dG·dC 11-mer duplex is shown in Supplementary Figure S3A. These phosphorus resonances have been assigned from an analysis of cross-peak patterns in a proton detected phosphorus−proton heteronuclear correlation experiment (Figure S3B). Each nonterminal phosphorus can be correlated with its 5′-linked H3′ proton (three-bond H−P coupling) and its 3′-linked H4′ proton (four-bond H−P coupling) in the two-dimensional contour plot of the adduct duplex (Figure S3B). The most downfield shifted phosphorus (−3.65 ppm) is assigned to the dG16-dC17 step on the unmodified strand with the phosphorus chemical shifts for the adduct duplex listed in the caption to Figure S3 and in Table S2.

Molecular Mechanics Computations. The search strategy employed began with a B-DNA (Arnott et al., 1976) central five base pair d(T4-C5-[MC]G6-C7-T8)·d(A15-G16-C17-G18-A19) segment of the (−)-*trans-anti*-[MC]dG·dC 11-mer duplex. The MC−DNA orientation space was searched with 16 energy minimization trials in which α′ ([MC]dG6(N^1)−[MC]dG6(C^2)−[MC]dG6(N^2)−MC(C^4)) and β′ ([MC]dG6-(C^2)−[MC]dG6(N^2)−MC(C^4)−MC(C^3)) were each started

Table 2: Comparison of Input Interproton Carcinogen−DNA Distance Bounds with Those Observed for the d(T4-C5-[MC]G6-C7-T8)·d(A15-G16-C17-G18-A19) Segment of the NMR Energy-Minimized Solution Structure of the (−)-*trans-anti*-[MC]dG·dC 11-mer Duplex

	interproton distances, Å	
	exptl bounds	obsd
Exchangeable Protons		
[MC]dG6(NH1)−MC(H2)	3.0−5.5	4.38
[MC]dG6(NH1)−MC(H3)	3.5−6.0	4.55
[MC]dG6(NH1)−MC(H4)	3.5−6.0	4.41
[MC]dG6(NH1)−MC(5-CH_3)	3.0−5.5	5.05[a]
[MC]dG6(NH2)−MC(H2)	2.5−5.0	2.96
[MC]dG6(NH2)−MC(H3)	2.5−5.0	3.43
[MC]dG6(NH2)−MC(H4)	3.0−5.5	2.86
[MC]dG6(NH2)−MC(5-CH_3)	2.5−5.0	4.10[a]
dG16(NH1)−MC(5-CH_3)	4.5−6.0	4.63[a]
dG18(NH1)−MC(H2)	3.0−5.5	4.63
dG18(NH1)−MC(H3)	3.5−6.0	5.55
Nonexchangeable Protons		
[MC]dG6(H1′)−MC(H3)	2.6−3.9	3.67
[MC]dG6(H1′)−MC(H4)	2.6−4.0	3.84
[MC]dG6(H1′)−MC(5-CH_3)	4.0−6.0	4.81[a]
dG16(H1′)−MC(H8)	4.0−6.0	5.85
dC17(H1′)−MC(H10)	2.9−4.3	3.57
dC17(H2″)−MC(H10)	3.2−4.8	4.51
dC17(H2″)−MC(H11)	3.0−4.5	4.29
dC17(H4′)−MC(H9)	2.4−3.6	2.89
dC17(H4′)−MC(H10)	2.7−4.0	2.48
dC17(H4′)−MC(H11)	2.8−4.2	3.79
dC17(H4′)−MC(H12)	3.1−4.6	5.69
dC17(H5′,H5″)−MC(H9)	3.0−5.0	3.53,[b] 2.84[b]
dG18(H1′)−MC(H12)	2.9−4.3	4.05
dG18(H3′)−MC(H12)	3.3−4.9	5.16
dG18(H4′)−MC(H10)	3.3−4.9	5.09
dG18(H4′)−MC(H11)	2.8−4.1	3.56
dG18(H4′)−MC(H12)	2.2−3.2	2.63
dG18(H5′,H5″)−MC(H11)	3.0−5.0	4.20,[b] 3.05[b]
dG18(H5′,H5″)−MC(H12)	2.5−4.5	4.47,[b] 3.76[b]

[a] Average value for the three methyl protons. [b] H5′ and H5″ protons are not stereospecifically assigned.

at 0°, 90°, 180°, 270° in all combinations, and the DNA starting conformation was the energy-minimized B form. Searching orientation space at 90° intervals of α' and β' is a robust procedure for locating all the important potential energy wells because our minimization protocol permits torsion angle variations of up to 100° in each minimization step (Hingerty et al., 1989). Consequently, energy minima in each quadrant of α' and β' are accessible, and the reduced variable domain of torsion angle space greatly enhances the likelihood of finding the important structures. In these trials, the DUPLEX hydrogen-bond penalty function (Hingerty et al., 1989) for Watson−Crick base pairing was utilized at all base pairs, since the NMR data indicated that the modified base pair was hydrogen-bonded, and NMR derived upper and lower bound distance restraints listed in Table 2 were included.

Of the 16 structures computed, twelve were identified as being in the family of structures in which the chrysenyl ring of the (−)-*trans-anti*-[MC]dG adduct is positioned in a B-DNA minor groove and oriented toward the 3′-direction of the modified strand. The pairwise RMS deviation of the d(T4-C5-[MC]G6-C7-T8)·d(A15-G16-C17-G18-A19) segment of these twelve structures ranges between 0.35 and 2.16 Å (mean pairwise deviation is 1.04 ± 0.44). Eight of these twelve structures exhibited the best fit to the NMR data as indicated by their corresponding goodness-of-fit values, F_N and F_{NN} for eqs 1 and 2, respectively, with W = 15 kcal/(mol·Å^2) (Materials and Methods section). Two views of the central pentanucleotide duplex segment showing the superposition of these eight structures are shown in Figure 6, panels A and B. The distribution of their sugar pseu-

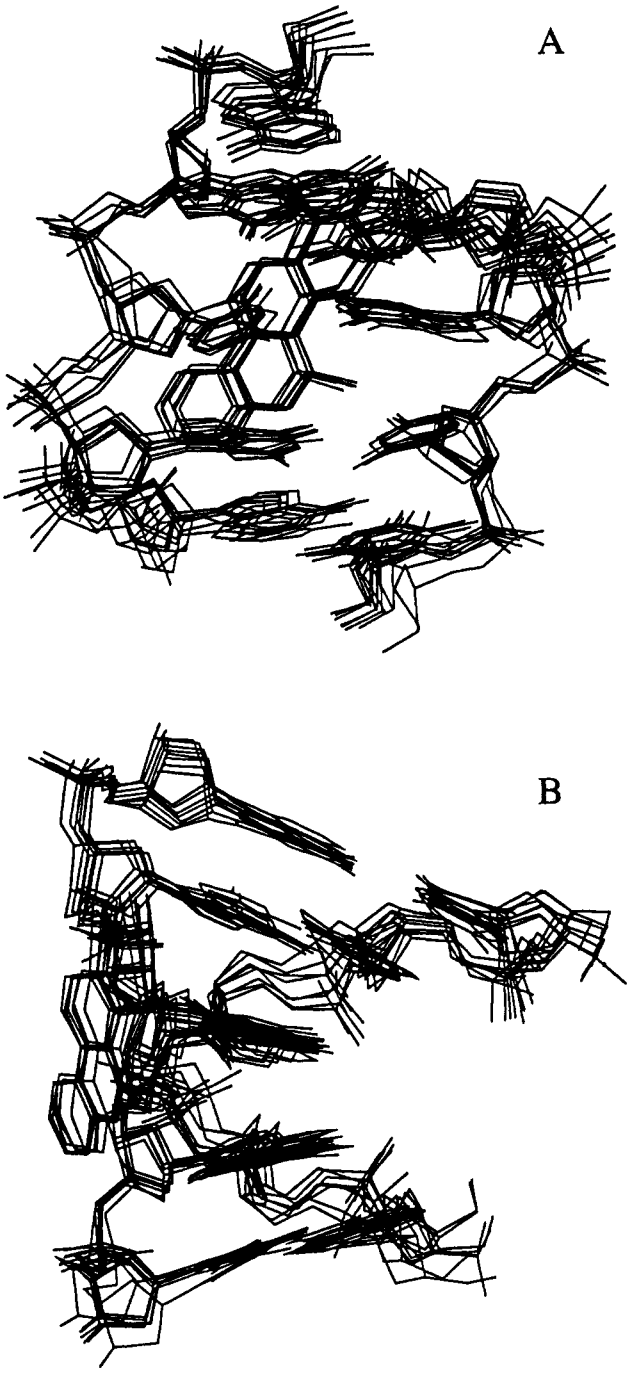

FIGURE 6: (A) View looking into the minor groove and (B) a side view rotated 90° of the eight superpositioned structures that best-fit the NMR data for the central d(T4-C5-[MC]G6-C7-T8)·d(A15-G16-T17-G18-A19) segment of the (−)-*trans-anti*-[MC]dG·dC 11-mer duplex obtained from the 16 trials to search conformational space using NMR restraints (Table 2) and the program DUPLEX. The relative goodness of fit to the NMR data was determined by evaluating eqs 1 and 2 (Materials and Methods section) for F_N and F_{NN}, which indicate the magnitude of the deviation of the distances in the model from the given upper and lower bounds, respectively, of the corresponding distance restraints. The structure with the lowest energy value (E = −227.3) also has the best goodness-of-fit function values (F_N = 15.1, F_{NN} = 2.0).

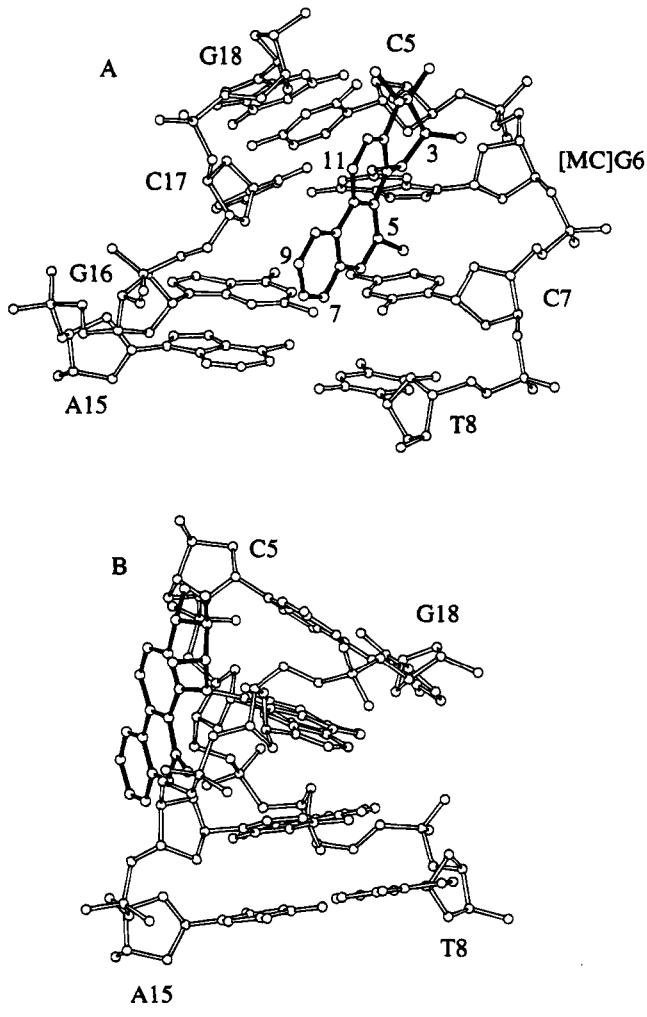

FIGURE 7: Views of the energy-minimized solution structure of the (−)-*trans-anti*-[MC]dG•dC 11-mer duplex. The 5-methylchrysenyl moiety is shown in darkened bonds. (A) A view looking into the minor groove of the d(C5-[MC]G6-C7-T8)•d(A15-G16-C17-G18) segment emphasizes the buckled and wedge-shaped geometry of the [MC]dG6•dC17 and dC7•dG16 base pairs. (B) A view rotated through 90° features the bend in the helix resulting from the wedging apart of the minor groove edges of the [MC]-dG6•dC17 and dC7•dG16 base pairs by the MC(5-CH_3) group. Figures were prepared using Molscript V1.1 (Kraulis, 1991).

dorotation (*P*) and glycosidic (χ) torsion angles for the central d(C5-[MC]G6-C7)•d(G16-C17-G18) residues are given in Supplementary Table S4. The lowest energy conformer (E = −227.3 kcal/mol) with the best goodness-of-fit indices (F_N and F_{NN} = 15.1 and 2.0, respectively, with W = 15 kcal/(mol•Å^2)) was embedded into an energy minimized B-form 11-mer. This 11-mer was reminimized with all restraints. Subsequently, the hydrogen-bond penalty function and the distance restraints were released with energy minimization in one step, yielding a final unrestrained structure.

Solution Structure. A view normal to the helix axis and looking into the minor groove of the d(C5-[MC]G6-C7-T8)•d(A15-G16-C17-G18) segment of the NMR energy-minimized structure of the (−)-*trans-anti*-[MC]dG•dC 11-mer duplex is shown in Figure 7A. The covalently linked 5-methylchrysenyl benzylic ring is positioned against the minor groove edges of the dC5 and [MC]dG6 residues on the modified strand of the adduct duplex, while the aromatic chrysenyl ring is positioned edgewise so that its MC(5-CH_3) and MC(H6) containing edge is oriented toward the floor of the minor groove. The 5-methyl group wedges between the [MC]dG6•dC17 and dC7•dG16 base pairs, thereby buckling the modified base pair by 22.2° without disruption of the Watson−Crick hydrogen-bonding alignment. The buckle and propeller twist angles of all eleven base pairs as well as the rise distances and twist angles along each DNA strand (computed using the method of Babcock et al., 1994) for the NMR energy-minimized structure of the adduct duplex are plotted in Supplementary Figure S4. An alternate view rotated through 90° of the d(C5-[MC]G6-C7-T8)•d(A15-G16-C17-G18) segment of the (−)-*trans-anti*-[MC]dG•dC 11-mer duplex (Figure 7B) shows that the insertion of the chrysenyl 5-methyl group wedges apart the minor groove edges of the [MC]dG6•dC17 and dC7•dG16 base pairs and concurrently narrows their major groove edges, resulting in a ~47° bend in the DNA helix. An approximately 0.5 Å increase in the rise distances is observed for the [MC]dG6-dC7 and dG16-dC17 steps (3.7 and 3.6 Å, respectively, Figure S4), and a slight unwinding of the helix is also observed between adjacent [MC]dG6•dC17 and dC7•dG16 base pairs (twist angle = 29.5°, Figure S4) in the NMR energy-minimized structure of the duplex adduct.

Two views of the d([MC]G6-C7)•d(G16-C17) segment of the (−)-*trans-anti*-[MC]dG•dC 11-mer duplex are shown in Figure 8, panels A and B, with the emphasis on the stacking interactions between the aromatic chrysenyl ring and DNA. One face of the 5-methylchrysenyl ring stacks over the minor groove edge of the dC17 located opposite the modification site, while the other face is exposed to solvent (Figure 8A). The benzylic ring is oriented toward the dC5-[MC]dG6 step on the modified strand while the aromatic chrysenyl ring points toward the dG16-dC17 step on the unmodified complementary strand in the structure of the adduct duplex. The NMR data indicate that the individual 5-methyl protons rotate rapidly about the methyl carbon (C^M) to the carbon in the ring (C^5) bond since a single resonance is observed at 2.45 ppm. In order for the 5-methyl group to rotate freely in the sterically crowded bay region, the aromatic chrysenyl ring is slightly distorted from planarity by −5.7° ($C^{4A}-C^{5A}-C^{5B}-C^{11}$ dihedral angle) and the 5-methyl group is positioned out of the plane of the chrysenyl ring by −9.2° ($C^7-C^6-C^5-C^M$ dihedral angle). These slight distortions away from planarity for the 5-methylchrysenyl ring are emphasized in the edge on view of the ring in Figure 8B. The benzylic ring adopts a distorted half-chair conformation with the MC(H1) and MC(H2) protons in a pseudodiaxial orientation while the MC(H3) and MC(H4) protons are in a pseudo-diequatorial orientation.

The carcinogen−base linkage site for the [MC]dG6 residue is defined by the angles α' ([MC]dG6(N^1)−[MC]dG6(C^2)−[MC]dG6(N^2)−MC(C^4)) = 176° and β' ([MC]dG6(C^2)−[MC]dG6(N^2)−MC(C^4)−MC(C^3)) = 63° in the NMR energy-minimized structure of the (−)-*trans-anti*-[MC]dG•dC 11-mer duplex. The glycosidic torsion angles, sugar puckers, and backbone torsion angles for the d(T4-C5-[MC]G6-C7-T8)•d(A15-G16-C17-G18-A19) segment of the (−)-*trans-anti*-[MC]dG•dC 11-mer duplex are listed in Supplementary Table S5. The pseudorotation parameter of dC7 is in the C1′-*exo* domain and that of dC17 is in the O4′-*endo* domain (Altona & Sundaralingam, 1972). The glycosidic torsion angle at the [MC]dG6 modification site adopts a high *anti* conformation with χ = 282° (Table S5). All remaining backbone torsion angles and sugar pseudorotation parameters

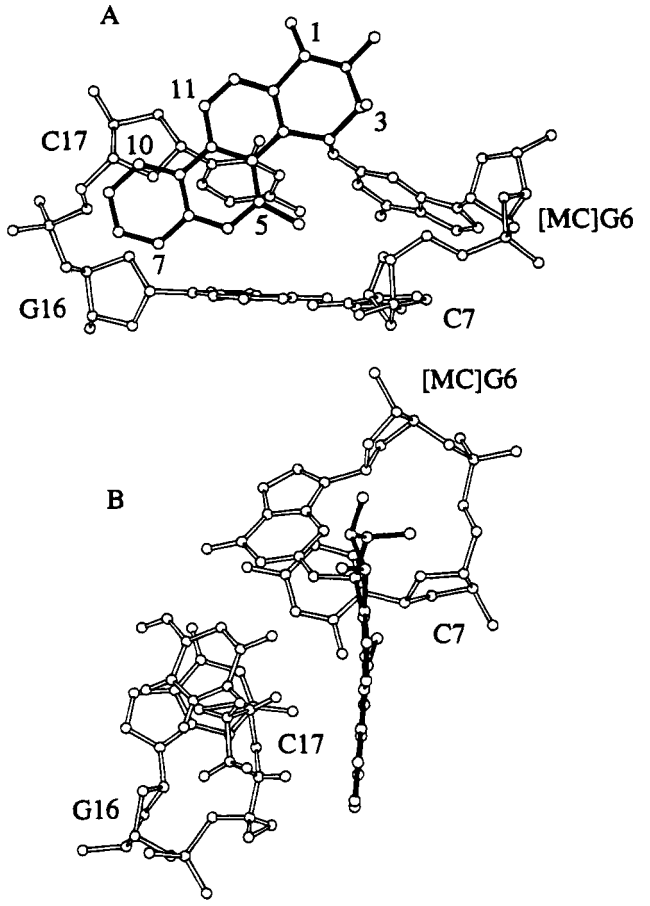

FIGURE 8: Views of the energy-minimized solution structure of the (−)-*trans-anti*-[MC]dG·dC 11-mer duplex. The 5-methylchrysenyl moiety is shown in darkened bonds. (A) A view looking into the minor groove of the d([MC]G6-C7)·d(G16-C17) segment emphasizing the stacking of the aromatic chrysenyl ring over the dC17 residue located on the unmodified strand. (B) A view rotated through 90° demonstrates the slight propeller-like distortion of the chrysenyl ring system and the out-of-plane 5-methyl group. Figures were prepared using Molscript V1.1 (Kraulis, 1991).

in the adduct duplex fall within or near the B_1-DNA conformation.

Convergence to very similar final structures resulted when the NMR-energy minimized structure was distorted by +45° or −45° at each of the two bonds (α′ and β′) at the base−carcinogen linkage and reminimized with restraints. Two views of the best fit superposition of the resulting four structures obtained from the distortion of α′ and β′ are plotted in Supplementary Figure S5.

DISCUSSION

Spectral Quality. Well-resolved imino (Figure 1A) and nonexchangeable (Figure 1B) proton resonances and partially resolved phosphorus resonances (Figure S3A) are observed for the (−)-*trans-anti*-[MC]dG·dC 11-mer duplex in aqueous solution. The NOE connectivities involving exchangeable protons (Figures 2 and 3) and nonexchangeable protons (Figure 4) can be readily followed in the NOESY data sets, thus permitting the assignment of nucleic acid (Tables 1, S1, and S2) and 5-methylchrysenyl (Figure 5) protons in the adduct duplex. In addition, a series of well-resolved carcinogen−DNA NOEs between the 5-methylchrysenyl and nucleic acid protons (numbered cross-peaks in Figures 2, 3 and 4) are observed and provide the restraints (Table 2) necessary for the alignment of the carcinogen along the helix. The one-dimensional (Figure 1) and two-dimensional exchangeable (Figures 2 and 3) and nonexchangeable (Figure 4) proton data are consistent with formation of a single conformation for the (−)-*trans-anti*-[MC]dG·dC 11-mer duplex in solution.

We note that the MC(H10) and MC(H11) protons which correspond to the 5-methylchrysenyl ring protons that resonate at lowest field (Figure 5) exhibit increased line widths (Figure 1B) in the nonexchangeable proton spectrum of the adduct duplex. This broadening could reflect small conformational interconversions involving the relative out-of-plane dispositions of the crowded MC(H10) and MC(H11) protons with respect to the plane of the chrysenyl ring in the (−)-*trans-anti*-[MC]dG·dC 11-mer duplex.

Minor Groove Alignment. The alignment of the 5-methylchrysenyl ring in the minor groove of the DNA helix is fully supported by the experimental carcinogen−DNA NOE data on the (−)-*trans-anti*-[MC]dG·dC 11-mer duplex (Table 2). The edge of the 5-methylchrysenyl ring extending from C^2 to C^5 is positioned toward the minor groove edge of the modified [MC]dC6 residue of the adduct duplex (Figure 7A). This alignment is supported by the carcinogen−DNA NOEs observed between the MC(H2), MC(H3), MC(H4), and MC-(5-CH_3) protons and the minor groove amino and sugar H1′ protons of [MC]dG6 in the adduct duplex (Table 2). The long edge of the chrysenyl ring extending from C^9 to C^{11} is positioned along the minor groove edge of dC17 on the unmodified strand in the solution structure of the adduct duplex (Figure 7A). This alignment is supported by the carcinogen−DNA NOEs observed between the MC(H9), MC(H10), and MC(H11) protons and the minor groove sugar H1′, H2″, and H4′ protons of dC17 in the adduct duplex (Table 2).

The aromatic chrysenyl ring is directed toward the 3′-end of the modified strand in the solution structure of the adduct duplex (Figure 7). This alignment is supported by the NOE between the MC(H8) proton located toward one end of the chrysenyl ring which is furthest from the covalent linkage site and the 3′-side dG16(H1′) proton (peak 2, Figure 4) and by the NOE between the MC(H12) proton located toward the opposite end of the ring and the 5′-side dG18(H1′) proton (peak 1, Figure 4).

The aromatic chrysenyl ring partially stacks over the minor groove sugar face of dC17 in the adduct duplex (Figure 8A), accounting for the large upfield shifts observed at the minor groove sugar H1′ (−1.72 ppm), H2″ (−0.61 ppm), and H4′ (−0.49 ppm) protons of dC17 (Table S3). Smaller upfield shifts are also observed at the major groove base H6 (−0.42 ppm) and H5 (−0.18 ppm) and sugar H3′ (−0.27 ppm) protons of dC17 on proceeding from the control to the adduct duplex (Table S3).

The [MC]dG6·dC17 Modified Pair. A Watson−Crick alignment is observed for the [MC]dG6·dC17 base pair in the solution structure of the adduct duplex consistent with the observed NOE between the imino proton of [MC]dG6 and the amino protons of dC17 (peaks A and A′, Figure 3A). This modified base pair is however buckled by 22.2° (Figure S3) associated with the insertion of the 5-methyl group on the chrysenyl ring at the [MC]dG6-dC7 and dG16-dC17 steps in the adduct duplex. Such a perturbation is accompanied by a high *anti* glycosidic angle for [MC]dG6 and an O4′-*endo* sugar pucker for dC17 in the structure of the adduct

duplex (Table S5). The steric crowding between the H4 benzylic and CH_3-5 chrysenyl protons in the bay region of the [MC]dG adduct is relieved by both small deviations from planarity of the chrysenyl ring and a small out-of-plane positioning of the CH_3-5 group (Figure 8B).

Insertion of the Chrysenyl CH_3-5 Group into the Helix. The base pairs in the central d(C5-[MC]G6-C7)•d(G16-C17-G18) segment of the adduct duplex adopt a right-handed helix alignment with Watson−Crick pairing at the dC5•dG18 and dC7•dG16 base pairs which flank the [MC]dG6•dC17 modification site. The hydrophobic 5-methyl group of the chrysene chromophore wedges between the [MC]dG6•dC17 and dC7•dG16 base pairs, resulting in an opening of the minor groove edge and a compression of the major groove edge at the opposing [MC]dG6-dC7 and dG16-dC17 steps on the modified and unmodified strands of the adduct duplex, respectively (Figure 7B). We detect shorter than normal interproton distances for the purine (H8)-3′−5′-pyrimidine (H5) steps at the wedge site consistent with compression of the major groove in the solution structure of the adduct duplex. These distances are 2.66 Å between the H8 of [MC]-dG6 and H5 of dC7 (corresponds to NOE cross-peak F, Figure 4) and 3.04 Å between the H8 of dG16 and the H5 of dC17 (corresponds to NOE cross-peak G, Figure 4). The resulting wedge-shaped alignment causes a 47° bend in the helix axis which is accompanied by a small unwinding (twist angle 29.5°, Figure S4) between the [MC]dG6•dC17 and dC7•dG16 base pairs.

Insertion of the hydrophobic 5-methyl group of chrysene into the helix should result in upfield shifts due to ring current effects from the base pairs at the wedge site in the structure of the (−)-*trans-anti*-[MC]dG•dC 11-mer duplex. The CH_3-5 proton chemical shift of 2.45 ppm in the adduct duplex is to high field of characteristic aromatic methyl proton shift values though the magnitude of the upfield shift is uncertain in the absence of a control value. We note, however, that the adjacent MC(H6) proton in the (−)-*trans-anti*-[MC]-dG•dC 11-mer duplex is upfield shifted by 1.5 ppm relative to its BP(H12) proton counterpart in the analogous (−)-*trans-anti*-[BP]dG•dC 11-mer duplex (Figure 5) where there is no insertion into the helix.

The wedge-shaped alignment between the [MC]dG6•dC17 pair and its dC7•dG16 3′-neighboring pair but not its dC5•dG18 5′-neighboring pair is manifested in distinct NOE patterns between these two steps in the (−)-*trans-anti*-[MC]-dG•dC 11-mer duplex. Thus, the weaker NOE between the imino protons of [MC]dG6 and dG16 (peak D, Figure 2A) relative to the NOE between the imino protons of [MC]dG6 and dG18 (peak E, Figure 2A) can be readily explained since these protons are separated by a larger distance in the former (4.26 Å) compared to the latter (3.16 Å) in the solution structure of the adduct duplex. Similarly, the NOE between the base proton to its 5′-flanking sugar H1′ proton is stronger for the dG16-dC17 step (boxed peak a, Figure 4) compared to the dC17-dG18 step (boxed peak b, Figure 4) consistent with the shorter separation in the former (3.68 Å) compared to the latter (4.25 Å) in the solution structure of the adduct duplex.

It could be argued that bending is difficult to identify in DNA using NMR approaches due to the inherent limitations associated with a method that monitors short range interactions involving proton pairs separated by <5.5 Å. This is indeed a problem in the solution structure determination of unmodified DNA duplexes but less so for adduct containing DNA duplexes where NOEs between the adduct and its local DNA environment can help define both the alignment of the adduct on the duplex and helical perturbations including bending at the adduct site.

Comparison of the Solution Structures of the (−)-trans-anti-[BP]dG•dC 11-mer and (−)-trans-anti-[MC]dG•dC 11-mer Duplexes. In order to understand how the presence of a bay region methyl group affects the solution structure of the (−)-*trans-anti*-[MC]dG adduct, it is useful to compare this structure with that of the previously studied benzo[*a*]-pyrenyl (−)-*trans-anti*-[BP]dG adduct (De los Santos et al., 1992). The [BP]dG adduct lacks a methyl group and has an additional aromatic ring, but otherwise has identical orientations and stereochemistry of the hydroxyl groups and protons attached to the benzylic ring as found in the [MC]-dG adduct. In addition, the DNA sequence context of both adduct duplexes and the binding configuration at the N^2-dG position are the same (10*R* in the case of the BP adduct and 4*R* in the case of the MC adduct).

Comparative views looking normal to helix axis of the NMR energy-minimized structures of the (−)-*trans-anti*-[BP]-dG•dC 11-mer (Figure 9A) and (−)-*trans-anti*-[MC]dG•dC 11-mer (Figure 9B) duplexes show that, in both cases, the (−)-*trans-anti* adduct resides in the minor groove of a minimally perturbed B-DNA helix with all the Watson−Crick base pairs intact. The aromatic (either pyrenyl or chrysenyl) ring stacks predominantely over the dC17 sugar residue on the unmodified strand and is directed toward the 3′-end of the modified strand. In addition, the benzylic ring pucker conformation is similar in both cases in that the BP-(H10)−BP(H9) or MC(H4)−MC(H3) proton pairs which occupy the same positions in the benzylic ring of each adduct are pseudo-diequatorial while BP(H8)−BP(H7) and MC-(H2)−MC(H1), which are also located in analogous positions, are pseudo-diaxial.

The presence of the methyl group in the (−)-*trans-anti*-[MC]dG•dC 11-mer duplex does, however, result in subtle differences in the alignment of the chrysenyl ring relative to its pyrenyl counterpart. The chrysenyl ring is oriented more edgewise in the minor groove so that its methyl containing edge is positioned toward the floor of the minor groove and is centered more about the [MC]dG6•dC17 base pair (Figure 9B) than the corresponding pyrenyl ring in the (−)-*trans-anti*-[BP]dG6 adduct (Figure 9A). We note that the α' and β' angles covalently linking the MC and dG6 residues adopt values of 176° and 63° in the (−)-*trans-anti*-[MC]dG•dC 11-mer duplex (this study) compared to their counterpart α' and β' values of 152° and 78° covalently linking the BP and dG6 residues in the (−)-*trans-anti*-[BP]-dG•dC 11-mer duplex (De los Santos et al., 1992). More importantly, the insertion of the 5-methyl group between the [MC]dG6•dC17 and dC7•dG16 base pairs in the 5-methyl-chrysenyl adduct results in a buckling of the modified base pair and a more pronounced bend in the helix (Figure 9B) relative to the case of the (−)-*trans-anti*-[BP]dG adduct, which lacks the corresponding methyl group (Figure 9A).

Comparisons with Conformations of Other PAH−DNA Adducts. Previously, we have studied the solution structures of seven PAH−DNA adducts derived from the binding of benzo[*a*]pyrenyl (BP) and benzo[*c*]phenanthrenyl (BPh) diol epoxides to DNA (Cosman et al., 1992, 1993a,b, 1994a,b, 1995; De los Santos, 1992). These studies have provided

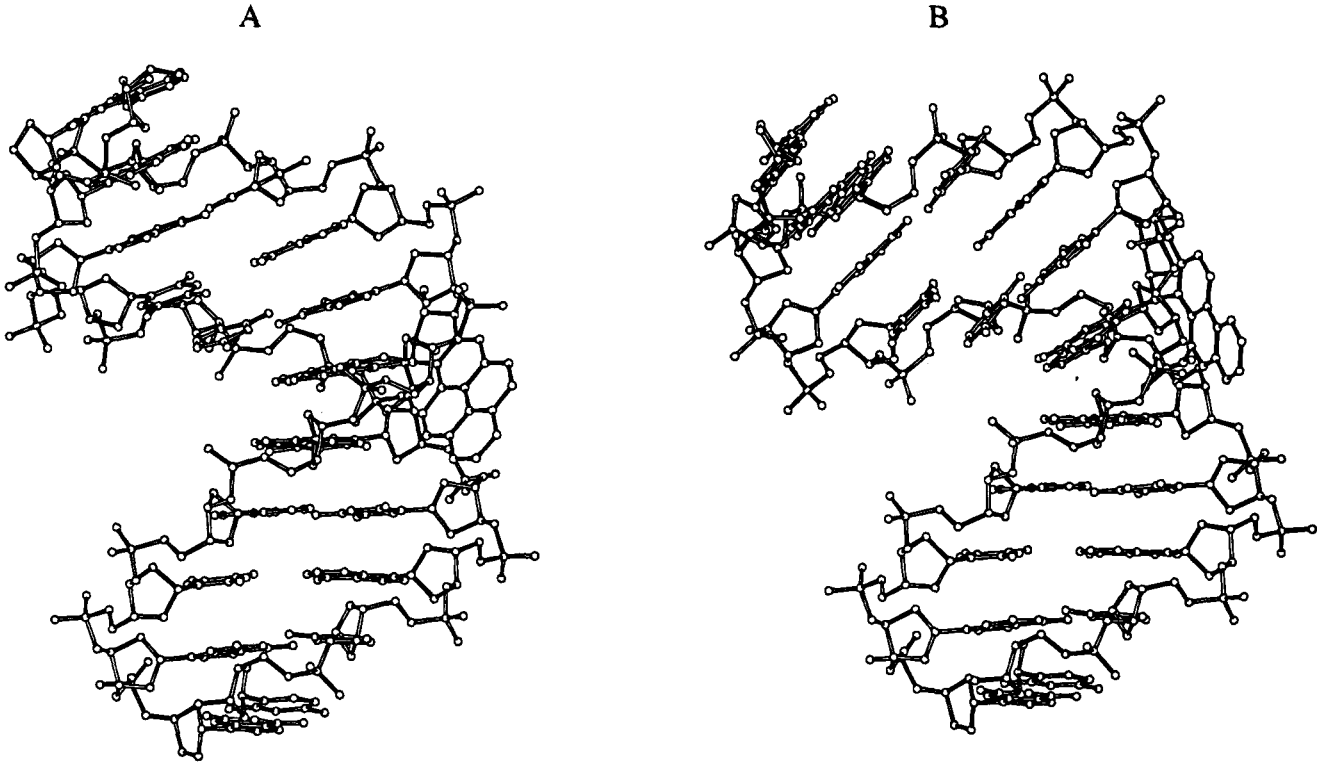

FIGURE 9: Comparative views normal to the helix axis of (A) the (−)-*trans-anti*-[BP]dG·dC 11-mer duplex and (B) the (−)-*trans-anti*-[MC]dG·dC 11-mer duplex. Although the aromatic (pyrenyl or chrysenyl) ring (shown in darkened bonds) points in the 3′-direction of the modified strand in both adducts, there is a more pronounced bend in the 5-methylchrysene modified duplex. Figures were prepared using Molscript V1.1 (Kraulis, 1991).

us with insights into how the conformation of the modified DNA is influenced by such factors as the stereochemistry of the PAH adduct, whether the modified base is positioned opposite a natural complementary base or a deletion site, and whether the location of the binding site is in the minor or major groove of the helix. Three families of PAH−DNA structures have been elucidated to date in which the adduct is either (1) positioned in the minor groove without significant distortion of the B-DNA duplex [(+)- and (−)-*trans-anti*-[BP]dG·dC 11-mer duplex] (Cosman et al., 1992; De los Santos et al., 1992), (2) intercalated into the helix by displacing the modified base [(+)-*cis-anti*-[BP]dG·dC 11-mer, and (+)-*trans*- and (+)-*cis-anti*-[BP]dG·del 11-mer duplexes] (Cosman et al., 1993a, 1994a,b), or (3) intercalated into the helix without disrupting the modified base pair [(+)- and (−)-*trans-anti*-[BPh]dA·dT 11-mer duplexes] (Cosman et al., 1993b, 1995). These conformational differences in turn may be related to the differences in the biological activities observed for the parent diol epoxides since the structure of the adduct may influence their interactions with repair and replication enzymes in the cell. The (−)-*trans-anti*-[MC]dG·dC 11-mer duplex belongs to the first family of structures outlined above, in which the chrysenyl ring is located in the minor groove and the Watson−Crick alignments of all eleven base pairs are intact. However, the presence of a methyl group in the bay region results in bending the DNA helix to a greater extent than previously observed.

Summary and Conclusions. The steric configurations of OH groups and the epoxide group in the bay region (reviewed by Conney, 1982) and the presence of a methyl group in the bay region (reviewed by Hecht et al., 1986) are two established factors which can influence the biological activities of bay region PAH diol epoxides. Our long-range goal is to systematically explore the conformational characteristics of the adducts formed when PAH diol epoxides with different structural and steric motifs, and of different mutagenic and tumorigenic activities, bind chemically to DNA. In this contribution, we have focused on the effects of a single methyl group in the bay region of (−)-*anti*-5-MeCDE on the structural features and alignment of the covalent *trans*-N^2-dG adducts in a DNA duplex; these observations are contrasted with those derived from the NMR characteristics of the stereochemically identical and structurally similar *trans*-N^2-dG adducts obtained from the reaction of (−)-*anti*-BPDE with DNA. The extra aromatic ring in the (−)-*trans-anti*-BPDE-N^2-dG lesions (the C^4 and C^5 atoms) is essentially furthest removed from nucleic acid moieties in oligonucleotide duplexes (Figure 9A; De los Santos et al., 1992); therefore, the effect of the 5-CH_3 group on the (−)-*trans-anti*-[MC]dG lesion structure can be evaluated. A new structural effect in which the methyl group is wedged between adjacent base pairs and causes a bend at the lesion site has been established here. While the effects of stereochemistry of diastereomeric and chiral PAH diol epoxides can be one important determinant of biological activity (reviewed by Conney, 1982), there is no doubt that the presence of (and the site of substitution) of a methyl group in stereochemically identical positional isomers can have a profound effect on the tumorigenic (Hecht et al., 1987) and mutagenic characteristics (Melikian et al., 1988; Amin et al., 1986, 1988) of diol epoxide derivatives in this family of chrysene compounds.

Enhanced tumorigenicity has been observed for a number of other PAH compounds in addition to chrysene when methylation occurs in a bay region; known examples include

methylphenanthrene (LaVoie et al., 1982), methylbenz[*a*]-anthracene (Wislocki et al., 1983), methylbenzo[*a*]pyrene (Iyer et al., 1980), and benz[*a*]anthracene (Slaga et al., 1979). The exact origin of this enhancement of the biological activities of the methylated PAH compounds is not known, but effects of structural perturbations by the bulky methyl group in the bay region is often suspected (Hecht et al., 1986). Indeed, the methyl group produces distortions from normal geometry in the sterically crowded region of 5-MeC; the bay region is somewhat widened and the methyl carbon atom is forced out of the plane of the aromatic ring system which itself is approximately planar (Kashino et al., 1984; Zacharias et al., 1984). However, these structural differences cannot yet be correlated with the biological effects of methyl substitution in the bay region. We have observed distortions from planarity of the aromatic chrysenyl ring in the (−)-*trans-anti*-[MC]dG adduct and a propeller-like distortion of the aromatic phenanthrenyl ring in both the (+)- and (−)-*trans-anti*-[BPh]dA adducts [derived from (+)- and (−)-*anti*-benzo[*c*]phenanthrene diol epoxide] (Cosman et al., 1993b, 1995) due to the highly strained fjord region found in this adduct. The results presented in this contribution on the solution structure of the (−)-*trans-anti*-[MC]dG•dC 11-mer duplex provide insight into the influence of a bay region methyl group on the characteristics of the adduct site: the hydrophobic methyl group decreases its exposure to the polar solvent by wedging into the helix. This insertion of the methyl group into the double helix results in a buckling of the modified base pair and in a bending of the helix. This distortion in the three-dimensional structure of the modified DNA, in turn, may distinctly affect the way that cellular enzymes can recognize and interact with these [MC]dG lesions in native DNA sequences.

While this work is entirely focused on the solution conformation of the (−)-*trans-anti*-[MC]dG•dC 11-mer duplex, analogous studies of the isomeric (+)-*trans-anti*-[MC]-dG•dC 11-mer duplex in solution are presently in progress. The differences in the structural characteristics of adducts derived from the binding of the highly tumorigenic (+)-*anti*-5-MeCDE and the weakly tumorigenic (−)-enantiomer to dG residues in DNA may eventually point the way to a deeper understanding of the relationships between adduct conformation and biological activity.

SUPPLEMENTARY MATERIAL AVAILABLE

Five tables listing the chemical shifts of the exchangeable protons and nonexchangeable protons of the entire adduct duplex, the chemical shift differences on adduct formation and backbone torsion angles of the energy-minimized structure for the central 5-mer segment, and the pseudorotation and glycosidic torsion angles of the central three base pairs for the 12 best fit structures; and five figures showing partial charges for the 5-methylchrysenyl moiety and N^2-dG linkage site, expanded phase-sensitive COSY and 50 ms mixing time NOESY contour plots of the 5-methylchrysenyl benzylic ring protons, a proton decoupled phosphorus spectrum and a proton−phosphorus correlation experiment, the helical parameters (twist, rise, buckle, propeller-twist) for the entire adduct duplex, and the superposition of four structures derived following energy minimization with restraints from the NMR energy-minimized structure in which the α' and β' angles were changed by ±45° (16 pages). Ordering information is given on any current masthead page.

REFERENCES

Altona, C., & Sundaralingam, M. (1972) *J. Am. Chem. Soc. 94*, 8205−8212.

Amin, S., Camanzo, J., Huie, K., & Hecht, S. S. (1984) *J. Org. Chem. 49*, 381−384.

Amin, S., Huie, K., Melikian, A. A., Leszcynska, J. M., & Hecht, S. S. (1985) *Cancer Res. 45*, 6406−6442.

Amin, S., Huie, K., Hecht, S. S., & Harvey, R. G. (1986) *Carcinogenesis 7*, 2067−2070.

Amin, S., Huie, K., Balanikas, G., & Hecht, S. S. (1988) *Carcinogeneis 9*, 2305−2308.

Amin, S., Misra, B., Braley, J., & Hecht, S. S. (1991) *Cancer Lett. 58*, 115−118.

Arnott, S., Bond, P. J., Selsing, E., & Smith, P. J. (1976) *Nucleic Acids Res. 2*, 2459−2470.

Babcock, M. S., Pednault, E. P. D., & Olson, W. K. (1993) *J. Biomol. Struct. Dyn. 11*, 597−628.

Bigger, C. A. H., Flickinger, D. J., Strandberg, J., Pataki, J., Harvey, R. G., & Dipple, A. (1990) *Carcinogenesis 12*, 2263−2265.

Brookes, P., Ellis, M. V., Pataki, J., & Harvey, R. G. (1986) *Carcinogenesis 7*, 463−466.

Conney, A. H. (1982) *Cancer Res. 42*, 4875−4917.

Cosman, M., Ibanez, V., Geacintov, N. E., & Harvey, R. G. (1990) *Carcinogenesis 11*, 1667−1672.

Cosman, M., de los Santos, C., Fiala, R., Hingerty, B. E., Singh, S., Ibanez, V., Margulis, L., Live, D., Geacintov, N. E., Broyde, S., & Patel, D. J. (1992) *Proc. Natl. Acad. Sci. U.S.A. 89*, 1914−1918.

Cosman, M., de los Santos, C., Fiala, R., Hingerty, B. E., Ibanez, V., Luna, E., Harvey, R., Geacintov, N. E., Broyde, S., & Patel, D. J. (1993a) *Biochemistry 32*, 4145−4155.

Cosman, M., Fiala, R., Hingerty, B. E., Laryea, A., Lee, H., Harvey, R., Amin, S., Geacintov, N. E., Broyde, S., & Patel, D. J. (1993b) *Biochemistry 32*, 12488−12497.

Cosman, M., Fiala, R., Hingerty, B. E., Amin, S., Geacintov, N. E., Broyde, S., & Patel, D. J. (1994a) *Biochemistry 33*, 11507−11517.

Cosman, M., Fiala, R., Hingerty, B. E., Amin, S., Geacintov, N. E., Broyde, S., & Patel, D. J. (1994b) *Biochemistry 33*, 11518−11527.

Cosman, M., Laryea, A., Fiala, R., Hingerty, B. E., Amin, S., Geacintov, N. E., Broyde, S., & Patel, D. J. (1995) *Biochemistry 34*, 1295−1307.

De los Santos, C., Cosman, M., Hingerty, B. E., Ibanez, V., Margulis, L., Geacintov, N. E., Broyde, S., & Patel, D. J. (1992) *Biochemistry 31*, 5245−5252.

Geacintov, N. E., Lee, M. S., Ibanez, V., Amin, S., & Hecht, S. S. (1990) *Carcinogenesis 11*, 985−989.

Hare, D. R., Wemmer, D. E., Chou, S. H., Drobny, G., & Reid, B. R. (1983) *J. Mol. Biol. 171*, 319−336.

Harvey, R. G. (1991) *Polycyclic Aromatic Compounds: Chemistry and Carcinogenicity*, Cambridge University Press, New York.

Harvey, R. G., Pataki, J., & Lee, H. (1986) *J. Org. Chem. 51*, 1407−1412.

Hecht, S. S., Bondelli, W. E., & Hoffman, D. (1974) *J. Natl. Cancer Inst. 53*, 1121−1133.

Hecht, S. S., LaVoie, E., Mazzarese, R., Amin, S., Bedenko, V., & Hoffman, D. (1978) *Cancer Res. 38*, 2191−2194.

Hecht, S. S., Rivenson, A., & Hoffman, D. (1980) *Cancer Res. 40*, 1396−1399.

Hecht, S. S., Radok, L., Amin, S., Huie, K., Melikian, A. A., Hoffman, D., Pataki, J., & Harvey, R. G. (1985) *Cancer Res. 45*, 1449−1452.

Hecht, S. S., Melikian, A. A., & Amin, S. (1986) *Acc. Chem. Res. 19*, 174−180.

Hecht, S. S., Amin, S., Huie, K., Melikian, A. A., & Harvey, R. G. (1987) *Cancer Res. 47*, 5310−5315.

Hingerty, B. E., & Broyde, S. (1985) *Biopolymers 24*, 2279−2299.

Hingerty, B. E., Figueroa, S., Hayden, T., & Broyde, S. (1989) *Biopolymers 28*, 1195−1222.

Iyer, R. P., Lyga, J. W., Secrist, J. A., III, Daub, G. H., & Slaga, T. J. (1980) *Cancer Res. 40*, 1073−1076.
Kashino, S., Zacharias, D. E., Prout, C. K., Carrell, H. L., & Glusker, J. P. (1984) *Acta Crystallogr. C40*, 536−540.
Kraulis, P. J. (1991) *J. Appl. Crystallogr. 24*, 946−950.
LaVoie, E. J., Bedenko, V., Tulley-Freiler, L., & Hoffmann, D. (1982) *Cancer Res. 42*, 4045−4049.
Lunde, G., & Bjorseth, A. (1977) *Nature 268*, 518−519.
Majumdar, A., & Hosur, R. V. (1992) *Prog. NMR Spectrosc. 24*, 109−158.
Marion, D., Ikura, M., Tschudin, R., & Bax, A. (1989) *J. Magn. Reson. 85*, 393−399.
Melikian, A. A., LaVoie, E. J., Hecht, S. S., & Hoffmann, D. (1982) *Cancer Res. 42*, 1239−1242.
Melikian, A. A., La Voie, E. J., Hecht, S. S., & Hoffman, D. (1983) *Carcinogenesis 4*, 843−849.
Melikian, A. A., Amin, S., Hecht, S. S., Hoffman, D., Pataki, J., & Harvey, R. G. (1984) *Cancer Res. 44*, 2524−2529.
Melikian, A. A., Amin, S., Huie, K., Hecht, S. S., & Harvey, R. G. (1988) *Cancer Res. 48*, 1781−1787.
Melikian, A. A., Prahalad, K. A., Amin, S., & Hecht, S. S. (1991) *Carcinogenesis 12*, 1665−1670.
Miller, E. C. (1978) *Cancer Res., 38*, 1479−1496.
Neidle, S., Subbiah, A., Kuroda, R., & Cooper, C. S. (1982) *Cancer Res. 42*, 3766−3768.
Norman, D., Abuaf, P., Hingerty, B. E., Live, D., Grunberger, D., Broyde, S., & Patel, D. J. (1989) *Biochemistry 28*, 7462−7476.
Ornstein, R. L., & Rein, R. (1979) *Biopolymers 18*, 1277−1291.
Pataki, J., Lee, H., & Harvey, R. G. (1983) *Carcinogenesis 4*, 399−402.
Patel, D. J., Kozlowski, S. A., Nordheim, A., & Rich, A. (1982) *Proc. Natl. Acad. Sci. U.S.A. 79*, 1413−1417.
Patel, D. J., Shapiro, L., & Hare, D. (1987) *Q. Rev. Biophys. 20*, 35−112.
Reardon, D., Prakash, A. S., Hilton, B. D., Roman, J. M., Pataki, J., Harvey, R. G., & Dipple, A. (1987) *Carcinogenesis 8*, 1317−1322.
Schlick, T., Hingerty, B. E., Peskin, C. S., Overton, M. L., & Broyde, S. (1990) in *Theoretical Chemistry and Molecular Biophysics* (Beveridge, D., & Lavery, R., Eds.) pp 39−58, Academic Press, New York.
Singer, B., & Grunberger, D. (1983) *Molecular Biology of Mutagens and Carcinogens*, Plenum Press, New York.
Singh, S. B., Hingerty, B. E., Singh, U. C., Greenberg, J. P., Geacintov, N. E., & Broyde, S. (1991) *Cancer Res. 51*, 3482−3492.
Sklenar, V., Miyashiro, H., Zon, G., Miles, H. T., & Bax, A. (1986) *FEBS Lett. 208*, 94−98.
Slaga, T. G., Gleason, G. L., DiGiovanni, J., Sukumaran, K. B., & Harvey, R. G. (1979) *Cancer Res. 39*, 1934−1936.
van de Ven, F. J., & Hilbers, C. W. (1988) *Eur. J. Biochem. 178*, 1−38.
Wise, S. A., Benner, B. A., Chesler, S. N., Hilpert, L. R., Vogt, C. R., & May, W. E. (1986) *Anal. Chem. 58*, 3067−3077.
Wislocki, P. G., Fiorentini, K. M., Fu, P. P., Yang, S. K., & Lu, A. K. H. (1983) *Carcinogenesis 2*, 215−217.
Xu, R. (1994) Ph.D. Dissertation, New York University.
Zacharias, D. E., Kashino, S., Glusker, J. P., Harvey, R. G., Amin, S., & Hecht, S. S. (1984) *Carcinogenesis 5*, 1421−1430.

BI942834Y